THE VERSATILITY OF THE ACOUSTO-OPTIC MEASURING PRINCIPLE IN CHARACTERIZING SOUND FIELDS

A Torras-Rosell DFM, Danish National Metrology Institute, Kongens Lyngby, Denmark
S Barrera-Figueroa DFM, Danish National Metrology Institute, Kongens Lyngby, Denmark
F Jacobsen Acoustic Technology, Technical University of Denmark, Kongens Lyngby, Denmark

1 INTRODUCTION

One of the typical problems in determining the quantities describing an acoustic field, e.g. sound pressure and particle velocity, is the influence of the transducer on the actual properties of sound to be measured when the transducer is immersed into the field. Typically, the influence of the transducer is either disregarded by assuming that the dimensions of the transducer are small compared with the wavelength of the sound wave, or subtracted by means of a transducer-based correction, typically in form of a frequency response, previously determined in a realization of an idealized sound field (e.g. free or diffuse field). Either solution introduces additional uncertainties to the measurement process, however quantifiable. Optical methods do not incur this problem because the "sensing" element is not a bulk transducer but a beam of light that does not change the properties of sound, thus giving the actual value of the acoustic quantities. Among the optical techniques used nowadays for characterizing sound fields, the acousto-optic effect, that is, the interaction between sound and light, has recently rendered promising results as a non-invasive measuring principle within the audible frequency range. When a laser beam travels through an acoustic field, it captures the properties of sound along the optical path and encodes this information into its phase as a line integral of the pressure. While this line integral does not provide a direct measure of the pressure distribution along the scanned line, there are ways to exploiting the potential of this measurement. This paper presents three different acoustic applications founded on the acousto-optic effect, namely the visualization of sound based on acousto-optic tomography, the localization of noise sources employing an acousto-optic beamformer, and the identification of acoustic sources using near-field acousto-optic holography. The theoretical aspects of each of these applications are underlined and supplemented with experimental results.

2 THE ACOUSTO-OPTIC EFFECT

The interaction between sound and light is in this paper only studied within the audible frequency range and under sound pressure levels below the threshold of pain. The former condition implies that diffraction effects can be disregarded from the physical description of the acousto-optic effect. This is not always the case at higher frequencies, in the ultrasonic domain. The latter condition makes it possible to relate the changes of refractive index of the medium, in this case air, to linear variations of the acoustic pressure. This simplifies the model used to couple the optical and acoustical properties of the medium significantly. Under the mentioned conditions, the refractive index can be written as follows,[1]

$$n \cong n_0 + \frac{n_0 - 1}{\gamma p_0} p\,, \tag{1}$$

where n_0 and p_0 are the refractive index and the atmospheric pressure under static conditions respectively, γ is the ratio of specific heats, and p is the acoustic pressure. Note that the second term on the right hand side of the previous equation, which represents the acousto-optic effect, is extremely small compared to n_0. For example, in air and under standard atmospheric conditions (p_0 = 101.3 kPa), a sound pressure of 1 Pa induces a variation of the refractive index that is nine orders of magnitude smaller than n_0. The characterization of acoustic fields by means of the acousto-optic

effect requires measuring such small changes of refractive index. By recalling that the speed of light is inversely proportional to the refractive index, the acousto-optic effect can be understood in this context as a modulation effect on the phase of light: the light travels slightly slower/faster when the acoustic pressure increases/decreases. This can in practice be detected using interferometry, and in particular, the experimental results presented in the following sections were carried out employing a laser Doppler vibrometer (LDV). Although this optical device is designed to measure mechanical vibrations, it can be shown that the output of a vibrometer whose laser beam is traveling through a sufficiently intense sound field and reflected off a surface with negligible vibrations corresponds to an apparent velocity such as,[1]

$$v_{LDV}(t) = \frac{n_0 - 1}{\gamma p_0 n_0} \frac{d}{dt}\left(\int_L p(\vec{r}, t)\, dl\right), \tag{2}$$

where L represents the path travelled by the light. This expression shows that the acoustic information captured by the LDV does not correspond to a direct measure of the pressure at a certain position, but to a line integral of the pressure along the path followed by the laser beam. The following sections illustrate three possible ways of exploiting this measurement principle for three different purposes.

3 ACOUSTIC IMAGING

Since the acousto-optic measuring principle does not provide a direct measure of the pressure but rather a measure of its line integral, the reconstruction of the actual pressure can be achieved using tomography and the Radon transform. The Radon transform of an acoustic field can simply be defined as the projection of the acoustic pressure into a set of parallel straight lines:

$$R_p(\theta, x', t) = \int_{-L/2}^{L/2} p(\vec{r}, t)\, dy'. \tag{3}$$

The sketch presented on the left hand side in Figure 1 illustrates the measurement principle as well as the system of coordinates used in this definition of the Radon transform. At this point, the apparent velocity presented in Eq. 2 can accordingly be reformulated as a function of the Radon transform of the acoustic field:

$$v_{LDV}(t) = \frac{n_0 - 1}{\gamma p_0 n_0} \frac{dR_p(\theta, x', t)}{dt}. \tag{4}$$

Thus, the Radon transform along a certain line can be determined by integrating the measured velocity in time:

$$\tilde{R}_p(\theta, x', t) = \frac{\gamma p_0 n_0}{n_0 - 1} \int v_{LDV}(t) dt. \tag{5}$$

The Radon transform is here denoted with a tilde to emphasize that it is a measured quantity, and thus, it is vulnerable to measurement noise. There is no need here to consider any integration constant, because such a constant (DC component in time) has no acoustic information. By measuring the acousto-optic effect over a sufficient number of angles of projection θ and a sufficient number of parallel line scans along the coordinate x', the original sound pressure distribution can be reconstructed using the inverse Radon transform.[2] This is in practice done with tomographic algorithms, which try to circumvent the problems arisen by the presence of extraneous noise during the measurement. The present work uses the so-called filtered back projection method, which is the most popular reconstruction algorithm in tomography for many fields of science. For a parallel line scanning configuration, this method estimates the pressure as follows,[2]

$$\tilde{p}(\vec{r}, t) = \int_0^{\pi} Q(\theta, x', t) d\theta, \tag{6}$$

where $Q(\theta, x', t)$ is the so-called "filtered projection":

$$Q(\theta, x', t) = \tilde{R}_p(\theta, x', t) * h(x'). \tag{7}$$

This "filtered projection" is simply the measured Radon transform convolved with a filter $h(x')$ that accounts for both the implementation of the reconstruction algorithm using the two-dimensional spatial Fourier transform (Ram-Lak filter) and the filtering imposed in the frequency domain in order to reduce the influence of noise outside of the frequency range of interest (e.g. a Cosine window). Generally speaking, the quality of the reconstruction is enhanced with increasing the total number of scans (the number of parallel lines times the number of angles of projection). It is recommendable to have as many angles of projection as parallel line scans approximately.[2]

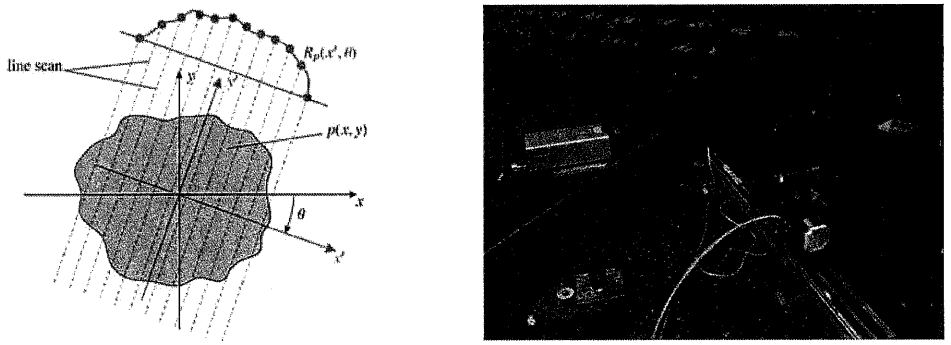

Figure 1: Sketch and measurement setup of the tomographic system.

The presented sound visualization technique is examined in the following for a measurement setup consisting of two loudspeakers whose centres were separated by 20 cm. The experiments were conducted in an anechoic room of about 1000 m^3. A picture of the experimental setup can be seen on the right hand side in Figure 1. The loudspeakers were mounted on two motors that made it possible to translate the speakers along the x' axis (from -0.45 to 0.45 m with a spatial resolution of 2.5 cm) and rotate them at different angles of projection (from 0 to 180 degrees with an angular resolution of 4.9 degrees approximately). A total of 1369 scans were performed. The measurement plane was located 5 cm above the loudspeakers. Note that the reflecting point where the laser was reflected off was continuously monitored with an accelerometer in order to ensure that mechanical vibrations were negligible.

The plot shown on the left hand side in Figure 2 presents the measured Radon transform when the loudspeakers were driven in phase with a 2.4 kHz pure tone. The plot shown on the right hand side in Figure 2 corresponds to the case where the loudspeakers were driven in antiphase.

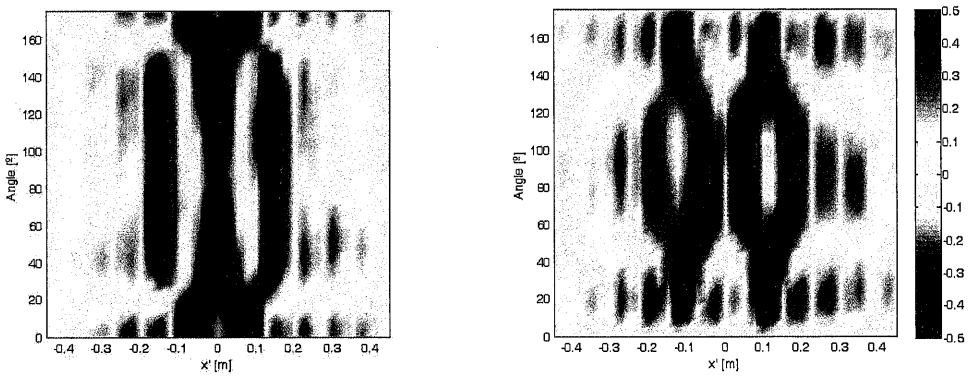

Figure 2: Instantaneous Radon transform measured with the LDV when the two loudspeakers were radiating in phase (on the left hand side) and in antiphase (on the right hand side). The measurement plane was located 5 cm above the speakers.

The respective even and odd symmetries of the measured Radon transforms are in good agreement with the nature of the sound fields under investigation, that is, two sound sources radiating in phase and in antiphase. The corresponding sound pressure maps reconstructed with the filtered back projection method are presented in Figure 3. As expected, the centres of the loudspeakers appear 20 cm apart from each other approximately, and the overall pressure distributions clearly illustrate whether the loudspeakers are driven in phase or in antiphase.

To further validate the quality of the reconstructions, measurements with a free field microphone were conducted at the same plane where the sound field was scanned with the LDV. For ease of comparison, a total of 1369 microphone positions were measured synchronously, yielding a virtual array of concentric circles. The results are shown in Figure 4. As can be seen, the pressure maps measured with the microphone compare well with the results obtained with the acousto-optic effect (cf. Figures 3 and 4). This demonstrates the potential of the presented acousto-optic tomography method, not only to visualize acoustic fields, but also to quantify them.

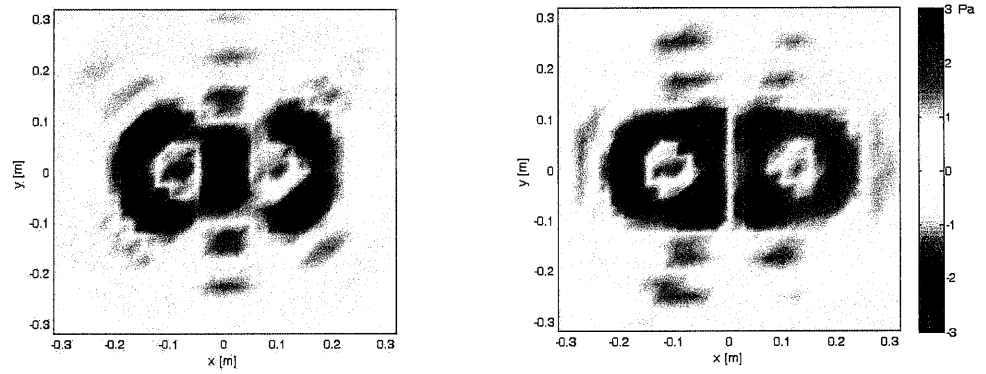

Figure 3: Instantaneous sound pressure reconstructed with the filtered back projection method when the two loudspeakers were radiating in phase (on the left hand side) and in antiphase (on the right hand side).

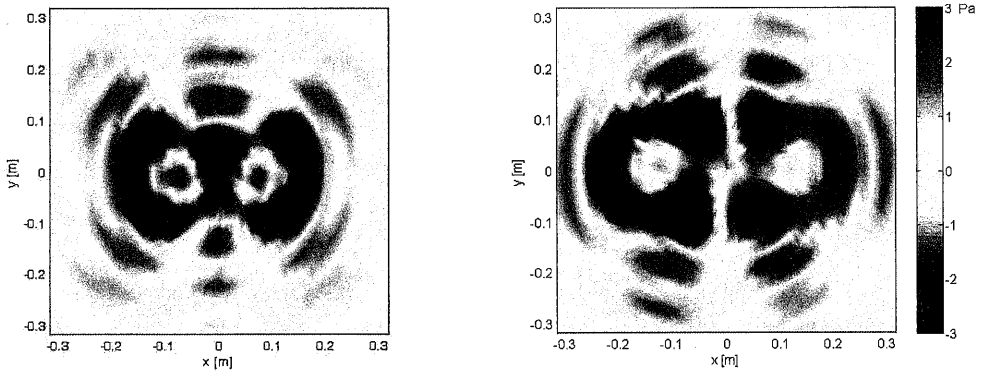

Figure 4: Sound pressure maps obtained with a free field microphone when the two loudspeakers were radiating in phase (on the left hand side) and in antiphase (on the right hand side).

4 SOURCE LOCALIZATION

Beamforming techniques are widely used in acoustics for the localization of sound sources in the far-field. This is a technique often based on microphone arrays that uses the phase mismatch among the sensors to identify the position of the acoustic sources. The performance of a beamforming technique can be assessed by means of the so-called resolution and maximum side lobe level. The optimization of these two parameters ensures that the beamforming system can

accurately separate two acoustic sources and that the output of the beamformer is not contaminated with ghost sources. There exists a great variety of approaches for enhancing the output of a beamforming system, e.g. by designing the layout of the array as well as the weighting functions of the sensors,[3,4] by mounting the sensors on a well-defined geometry such as a sphere that makes it possible to take advantage of the decomposition of the sound field into a set of orthogonal functions,[5,6] or by using deconvolution techniques at a post-processing stage to clean the measured beamforming map.[7] However, a common problem that cannot be overcome by any conventional beamforming technique is spatial aliasing. As a consequence, beamforming systems can only be used up to a certain frequency that is characteristic of each beamformer, though easily predictable by means of the Nyquist theorem when the spacing between transducers is constant. Just as in digital signal processing, where the signals sampled in time can yield temporal aliasing, spatial aliasing arises from the fact that the array used to measure the acoustic field consists of a finite number of microphones, thus sampling the acoustic field with a finite spatial resolution. This can for instance be illustrated with the beamforming output of a line array of microphones based on classical delay and sum beamforming,[3]

$$b_{DSB}(\theta) = \sum_{m=1}^{M} \tilde{p}_m \, e^{-jkmd\sin\theta} \tag{8}$$

where $\tilde{p}_m$ is the complex pressure of the m'th microphone, M is the total number of microphones, k is the wavenumber, d is the spacing between transducers and $e^{-jkmd\sin\theta}$ is the phase shift introduced to the m'th microphone in order to compensate for the delay experienced by the incident waves coming from the direction θ.Note that when θ equals zero, the beamforming output simply consists on the summation of pressures of the line array, and mathematically speaking, spatial aliasing comes from this finite summation of pressures. In theory, there would not be spatial aliasing if the line array consisted of an infinity number of microphones placed infinitely close to each other,

$$\lim_{\substack{M\to\infty \\ d\to 0}} \sum_{m=1}^{M} \tilde{p}_m \, d = \int_L P(\vec{r},\omega)dl, \tag{9}$$

where $\boldsymbol{L}$ represents here the straight line where the line array is located. This is of course not possible in reality, but the continuous line integral of the sound pressure can in fact be measured with an LDV whose laser beam travels along $\boldsymbol{L}$. By taking the temporal Fourier transform of the apparent velocity of the LDV presented in Equation (2),

$$V_{LDV}(\omega) = j\omega \frac{n_0 - 1}{\gamma p_0 n_0} \left(\int_L P(\vec{r},\omega)dl \right), \tag{10}$$

the following beamforming output can be defined based on the information captured with acousto-optic effect:[8]

$$b_{AO} = \left| \frac{1}{L} \int_L P(\vec{r},\omega)dl \right|^2 = \left| \frac{1}{L} \frac{\gamma p_0 n_0}{n_0 - 1} \frac{V_{LDV}(\omega)}{j\omega} \right|^2. \tag{11}$$

Figure 5 shows a sketch of the measuring principle as well as a picture of the experimental setup used to validate the presented acousto-optic beamformer. The measurements were carried out in the same anechoic room mentioned in the previous section. A loudspeaker was located 5 m away from the beamforming system to ensure the far-field condition. The loudspeaker was excited with a broad band signal that covered the entire audible frequency range. The acousto-optic beamformer was mounted on a turntable that made it possible to steer the system into different looking directions. All the equipment was covered with absorbing material to reduce the scattering effects at high frequencies. The assumption that the LDV was mainly measuring the acousto-optic effect instead of mechanical vibrations was regularly monitored with an accelerometer that was attached on the surface where the laser was reflected off.

The beamforming map obtained with the acousto-optic measuring principle can be seen on the left hand side in Figure 6. For ease of comparison, the same measurements were repeated with a line array of 19 microphones using the delay and sum beamforming technique. The corresponding results can be seen on the right hand side of Figure 6. As can be seen both beamforming patterns are fairly similar below 9 kHz approximately. As usual, the lower frequencies are more difficult to resolve due to the tendency of the beamforming algorithm to become more omnidirectional towards the low frequencies. Above 9 kHz, the results obtained with the delay and sum beamforming technique are contaminated with ghost sources that are caused by spatial aliasing. This is not a problem for the proposed acousto-optic beamformer, which indeed can cover the entire audible frequency range without traces of spatial aliasing. Note that the noise observed on the acousto-optic beamforming map below 2 kHz was mainly induced by the mechanical vibrations of the structure where the beamforming system was mounted. However, the overall performance of the acousto-optic beamformer proved the applicability of the proposed measurement principle to sound source localization.

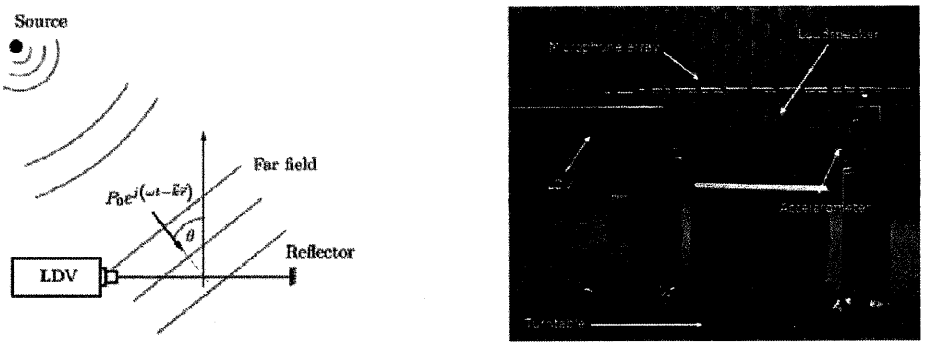

Figure 5: Sketch and experimental setup of the acousto-optic beamformer.

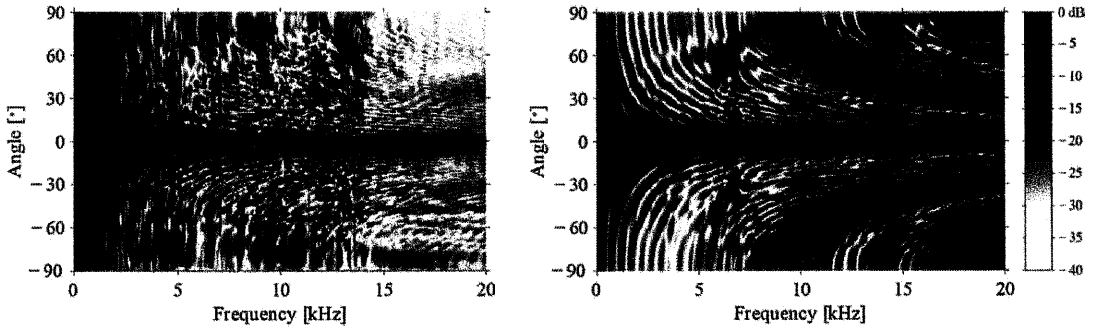

Figure 6: Beamforming results. On the left hand side, the map obtained with the acousto-optic beamformer. On the right hand side, the results achieved with a line arrays of 19 microphones.

5 ACOUSTIC HOLOGRAPHY

This section describes how to use the acousto-optic effect not to reconstruct the sound pressure on a measurement plane as presented in section 3, but to predict any acoustic property of a sound source on a parallel plane, different from the one where the acousto-optic effect is in fact measured. Such a measurement technique has been already developed for transducer arrays since the early 80's, under the name of near-field acoustic holography (NAH).[9-11] The power of this sound source identification technique lies on the fact that it is capable of reconstructing an entire acoustic field, that is, sound pressure, particle velocity and sound intensity, over a three-dimensional space, based on a two-dimensional measurement. Nowadays, there are several methods to implement NAH, e.g. Fourier-based NAH,[9-11] statistically optimized NAH (SONAH),[12] and the equivalent source method.[13] In the following, the conventional Fourier-based NAH method is adapted by means of the Fourier

slice theorem to make it possible to exploit the acousto-optic effect for holography purposes. Fourier-based NAH bases all its calculations on the wavenumber spectrum, that is, the two-dimensional spatial Fourier transform of the acoustic quantities captured on the measurement plane, typically referred to as hologram. The Fourier slice theorem states that the diagonals of the wavenumber spectrum are connected to the Radon transform of the measured acoustic field by means of a one-dimension spatial Fourier transform. Each of these diagonals is directly related to an angle of projection of the Radon transform, see Figure 7.

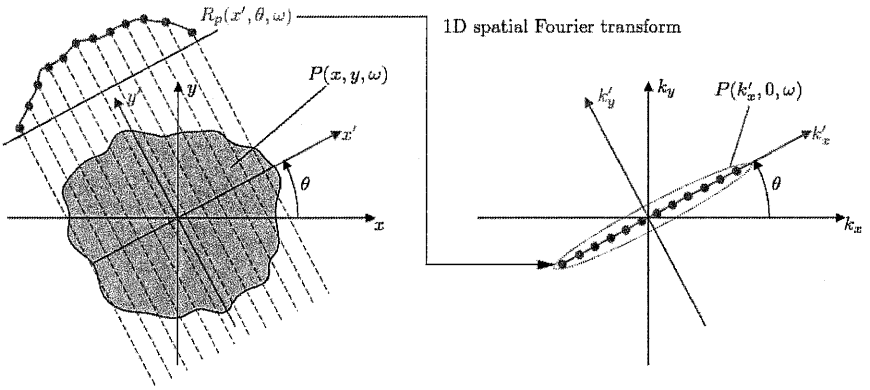

Figure 7: The Fourier slice theorem established the relationship between the Radon transform and diagonals of the wavenumber spectrum.

The proposed holographic method, denoted as near-field acousto-optic holography (NAOH) from now on, uses the apparent velocity of the LDV captured on the hologram plane to compute the diagonals of the wavenumber spectrum. This yields a sampling pattern on the wavenumber domain consisting on data points arranged in concentric circles as illustrated in Figure 8. Unlike the sampling pattern obtained with conventional NAH, where all the data points are uniformly distributed, NAOH presents a higher concentration of points towards the centre of the wavenumber domain (cf. the two examples shown in Figure 8). This is seen as a very interesting and beneficial feature, because Fourier-based NAH usually requires to filter out (regularise) the high spatial frequency components of the spectrum, in order to prevent the noise from dominating the reconstruction process when back-projecting the hologram to the prediction plane. NAOH has either no data points or a lower concentration of them than conventional techniques at these critical spatial frequencies. In short, the proposed NAOH method estimates the wavenumber spectra of the sound pressure and the particle velocity at the prediction plane ($z = z_s$) as follows,[14]

$$\begin{aligned} P_s(k_x, k_y, \omega) &= P_h(k_x, k_y, \omega) \cdot G_p = F^{\theta}_{x'}\{\tilde{R}_p(\theta, x', \omega)\} \cdot e^{jk_z(z_s - z_h)}, \\ V_s(k_x, k_y, \omega) &= P_h(k_x, k_y, \omega) \cdot G_v = F^{\theta}_{x'}\{\tilde{R}_p(\theta, x', \omega)\} \cdot \frac{k_z}{\rho_0 ck} e^{jk_z(z_s - z_h)}, \end{aligned} \tag{12}$$

where $F^{\theta}_{x'}\{\tilde{R}_p(\theta, x', \omega)\}$ denotes the one dimensional Fourier transform along the x'-axis of the Radon transform measured at the hologram plane ($z = z_h$), G_p and G_v represent the so-called pressure and velocity propagators, ρ_0 is the static density of the medium, c is the speed of sound, and k_z equals $\sqrt{k^2 - k_x^2 - k_y^2}$. Note that the propagators are defined in the same way as in Fourier-based NAH. The only difference is the exact values of k_z, which basically depend on the sampling points k_x and k_y in the wavenumber domain.

In order to validate the proposed method, the Radon transforms measured in Figure 2 (see section 3) were propagated to a new plane located 3 cm above the loudspeakers (the hologram was thus back-propagated 2 cm). The resulting sound pressures can be seen in Figure 9. As expected, the overall pressure distributions are fairly similar to the ones presented at the hologram (see Figure 3), but the overall energy of the reconstructed aperture is larger due to the fact that the prediction plan is closer to the sound sources. The validity of the proposed method was further confirmed by

comparing these results to reconstructions based on acousto-optic tomography of the very same sound field directly measured at the prediction plane. The results are presented in Figure 10. As can be seen, the agreement between the pressures predicted with the NAOH method and the acousto-optic tomography method is very good. It is worth mentioning that the NAOH method has not required the use of any regularization technique in order to stabilise the results. Although the signal-to-noise ratio was good during the measurements, the unique spectral features of the NAOH method further reduce the influence of extraneous noise at high spatial frequencies. Besides, with the presented NAOH method, it is also possible to estimate the particle velocity and the acoustic

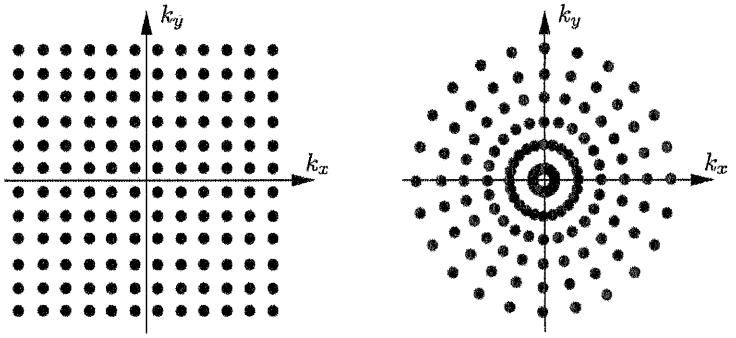

Figure 8: Data points sampled in the wavenumber domain when using conventional NAH (on the left hand side) and when using NAOH (on the right hand side).

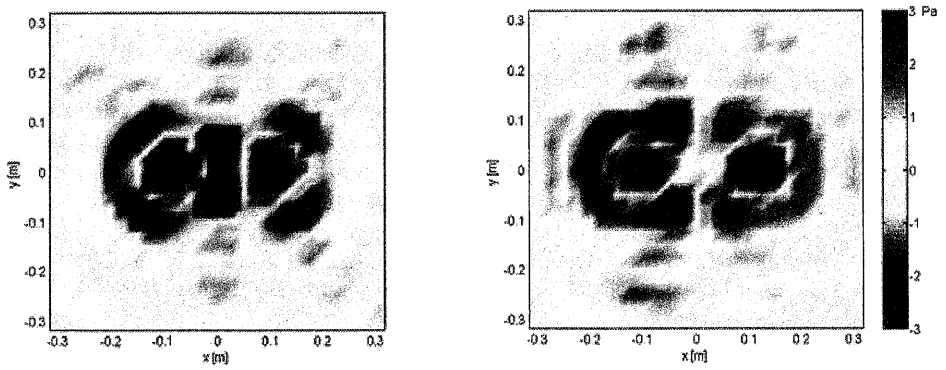

Figure 9: Instantaneous sound pressure estimated with NAOH on the prediction plane when the two loudspeakers are driven in phase (on the left hand side) and in antiphase (on the right hand side). The hologram and prediction planes were located 5 and 3 cm respectively above the loudspeakers.

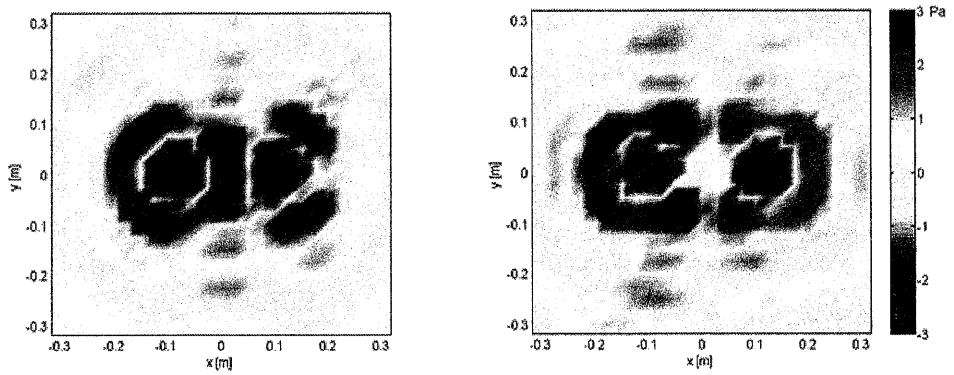

Figure 10: Instantaneous sound pressure distribution reconstructed with acousto-optic tomography from measurements taken directly on the prediction plan (3 cm above the loudspeakers). The loudspeakers were driven in phase (on the left hand side) and in antiphase (on the right hand side).

intensity of a sound field, thus giving a complete insight of the sound properties radiated by an acoustic source using the acousto-optic effect.

6 CONCLUSIONS

The present paper describes the versatility of the acousto-optic measuring principle for three different acoustic applications: visualization, localization and identification of acoustic sources. Each of these applications benefits from different measurement techniques (tomography, beamforming and holography) that are especially adapted to exploit different properties of the acousto-optic effect. The results achieved with the acousto-optic measuring principle are in good agreement with results obtained with conventional techniques based on microphone measurements. This proves that the acousto-optic effect is not only a measuring principle that can provide a qualitative description of an acoustic field, but it can also characterize an acoustic field quantitatively to a surprisingly good extent if we take into account that the instrumentation used to measure this phenomenon is not design for this purpose. In addition to that, the acousto-optic measuring principle renders unique properties that cannot be achieved with conventional techniques: it is a non-invasive technique, it is immune to spatial aliasing in beamforming applications and it provides unique spectral properties that soften the need for regularization techniques in holographic applications. All in all, it seems plausible that the acousto-optic effect may have an important role on the future of acoustic measurements within the audible frequency range.

7 REFERENCES

1. A. Torras-Rosell, S. Barrera-Figueroa and F. Jacobsen, 'Sound field reconstruction using acousto-optic tomography', J. Acoust. Soc. of Am. 131(5) 3786-3793 (2012).
2. A. C. Kak and M. Slaney. Principles of Computerized Tomographic Imaging, IEEE, New York (1988).
3. D. H. Johnson and D. E. Dudgeon. Array Signal Processing: Concepts and Techniques. Prentice-Hall, Englewood Cliffs, NJ (1993).
4. B. D. V. Veen and K. M. Buckley, 'Beamforming: A versatile approach to spatial filtering', IEEE ASSP Magazine 5(2) 4–24 (1988).
5. B. Rafaely, 'Plane-wave decomposition of the sound field on a sphere by spherical convolution', J. Acoust. Soc. of Am. 116(4) 2149–2157 (2004).
6. E. Tiana-Roig, F. Jacobsen, and E. Fernandez-Grande, 'Beamforming with a circular microphone array for localization of environmental noise sources', J. Acoust. Soc. of Am. 128(6) 3535–3542 (2010).
7. E. Tiana-Roig and F. Jacobsen, Acoustical source mapping based on deconvolution approaches for circular microphone arrays, Proc. 40th International Congress and Exposition on Noise Control Engineering, Osaka (2012).
8. A. Torras-Rosell, S. Barrera-Figueroa and F. Jacobsen, 'An acousto-optic beamformer', J. Acoust. Soc. of Am. 132(1) 144-149 (2012).
9. E. G. Williams, J. D. Maynard, and E. Skudrzyk, 'Sound source reconstructions using a microphone array', J. Acoust. Soc. of Am. 68(1) 340-344 (1980).
10. J. D. Maynard, E. G. Williams, and Y. Lee,, 'Nearfield acoustic holography I: Theory of generalized holography and the development of NAH', J. Acoust. Soc. of Am. 78(4) 1395-1413 (1985).
11. E. G. Williams. Fourier Acoustics: Sound radiation and Nearfield Acoustical Holography, Academic Press, San Diego (1999).
12. J. Hald, 'Basic theory and properties of statistically optimized near-field acoustical holography', J. Acoust. Soc. of Am. 125(4) 2105-2120 (2009).
13. A. Sarkissian, 'Method of superposition applied to patch near-field acoustic holography', J. Acoust. Soc. of Am. 118(2) 671-678 (2005).
14. A. Torras-Rosell, E. Fernandez-Grande, S. Barrera-Figueroa and F. Jacobsen, Investigating the use of the acousto-optic effect for acoustic holography, Proc. 41st International Congress and Exposition on Noise Control Engineering, New York (2012).